Article

Molecular Cell

m^{6}A Facilitates eIF4F-Independent mRNA Translation

Graphical Abstract

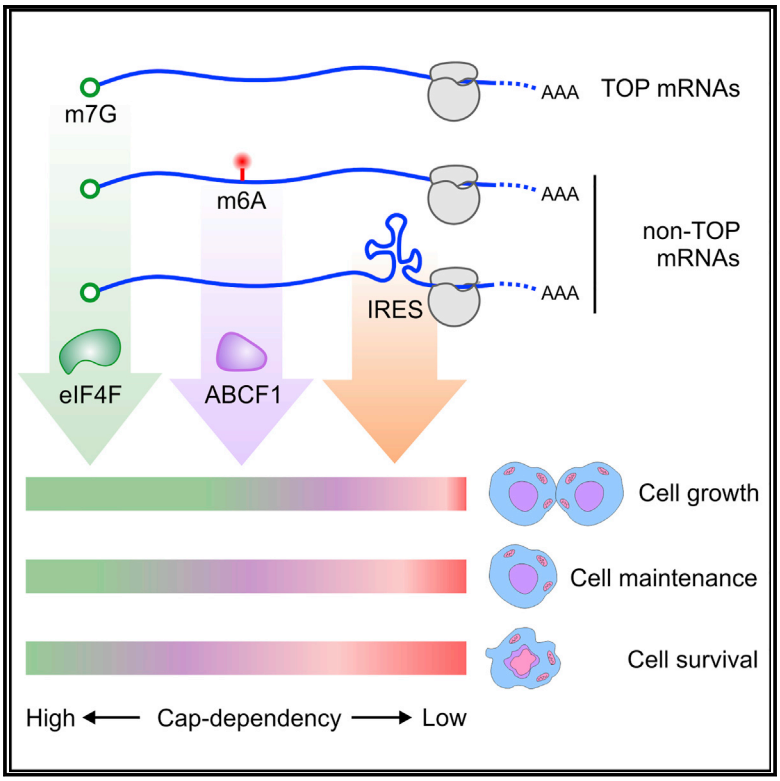

Authors

Ryan A. Coots, Xiao-Min Liu, Yuanhui Mao, ..., Ji Wan, Xingqian Zhang, Shu-Bing Qian

Correspondence

sq38@cornell.edu

In Brief

Coots et al. show that eIF4F inhibition partially represses global protein synthesis. m^{6}A in the 5′ UTR facilitates eIF4F-independent mRNA translation, and ABCF1 appears to be critical for m^{6}A-facilitated mRNA translation. These differential translation modes are coordinated in response to environmental perturbations.

Highlights

- eIF4F inhibition partially represses global protein synthesis
- Translation of non-TOP mRNAs depends on 5′ UTR *N*^{6}-methyladenosine
- ABCF1 is critical for eIF4F-independent mRNA translation
- ABCF1 coordinates with METTL3 in m^{6}A-facilitated mRNA translation

Coots et al., 2017, Molecular Cell *68*, 504–514
November 2, 2017
https://doi.org/10.1016/j.molcel.2017.10.002

CellPress

Molecular Cell
Article

m^{6}A Facilitates eIF4F-Independent mRNA Translation

Ryan A. Coots,[1,2,3] Xiao-Min Liu,[1,3] Yuanhui Mao,[1] Leiming Dong,[1] Jun Zhou,[1] Ji Wan,[1] Xingqian Zhang,[1] and Shu-Bing Qian[1,2,4,*]
[1]Division of Nutritional Sciences
[2]Graduate Field of Nutritional Sciences
Cornell University, Ithaca, NY 14853, USA
[3]These authors contributed equally
[4]Lead Contact
*Correspondence: sq38@cornell.edu
https://doi.org/10.1016/j.molcel.2017.10.002

SUMMARY

In eukaryotic cells, protein synthesis typically begins with the binding of eIF4F to the 7-methylguanylate (m^{7}G) cap found on the 5′ end of the majority of mRNAs. Surprisingly, overall translational output remains robust under eIF4F inhibition. The broad spectrum of eIF4F-resistant translatomes is incompatible with cap-independent translation mediated by internal ribosome entry sites (IRESs). Here, we report that *N*^{6}-methyladenosine (m^{6}A) facilitates mRNA translation that is resistant to eIF4F inactivation. Depletion of the methyltransferase METTL3 selectively inhibits translation of mRNAs bearing 5′ UTR methylation, but not mRNAs with 5′ terminal oligopyrimidine (TOP) elements. We identify ABCF1 as a critical mediator of m^{6}A-promoted translation under both stress and physiological conditions. Supporting the role of ABCF1 in m^{6}A-facilitated mRNA translation, ABCF1-sensitive transcripts largely overlap with METTL3-dependent mRNA targets. By illustrating the scope and mechanism of eIF4F-independent mRNA translation, these findings reshape our current perceptions of cellular translational pathways.

INTRODUCTION

Eukaryotic cells primarily employ a cap-dependent mechanism to initiate translation for the majority of mRNAs (Gebauer and Hentze, 2004; Hinnebusch, 2014; Jackson et al., 2010). The 5′ end of eukaryotic mRNAs is modified with a m^{7}G cap structure, which is recognized by an eukaryotic initiation factor 4E (eIF4E). eIF4E forms the eIF4F complex by binding to eIF4G (a scaffold protein) and eIF4A (a helicase) (Gross et al., 2003; Marintchev et al., 2009; Schütz et al., 2008). The cap recognition determines which mRNAs are to be translated and is subject to regulation by eIF4E-binding proteins (4E-BPs). When hypophosphorylated, 4E-BPs outcompete eIF4G for a binding site on eIF4E and prevent eIF4F assembly at the 5′ end of transcripts (Pause et al., 1994). One major signaling pathway that phosphorylates 4E-BPs is the mammalian target of rapamycin complex 1 (mTORC1) (Ma and Blenis, 2009; Zoncu et al., 2011). By sensing extracellular signals as well as the intracellular energy status, activated mTORC1 phosphorylates 4E-BPs that dissociate from eIF4E, thereby promoting eIF4F complex assembly (Sonenberg and Hinnebusch, 2009). Despite this well-established regulatory mechanism, in many cell lines, mTORC1 inhibition has only modest effects on the rate of protein synthesis (Beretta et al., 1996; Choo et al., 2008). The simplest interpretation of this conundrum is that cells rely on a cap-independent mechanism for a substantial amount of mRNA translation.

Cap-independent translation occurs during normal cellular processes (e.g., mitosis and apoptosis) or when the cap-dependent translation machinery is compromised by either stress or disease (Sonenberg and Hinnebusch, 2007). The best-characterized cap-independent initiation mechanisms involve internal ribosome entry sites (IRESs) (Hellen and Sarnow, 2001). Discovered in picornavirus mRNAs, the IRES element in the 5′ untranslated region (5′ UTR) forms a complex secondary structure capable of recruiting the translation machinery in the absence of some or even all initiation factors. A growing body of evidence suggests that certain cellular mRNAs may use the similar IRES mechanism for cap-independent translation initiation (Gilbert et al., 2007). Systematic approaches have been elaborated to identify putative IRES elements in human and viral genomes (Weingarten-Gabbay et al., 2016). Despite their capability of internal initiation, it is unclear whether these events truly occur within the original sequence context under physiological conditions. In fact, many cellular mRNAs that have been considered to contain IRESs failed to pass through stringent tests for internal initiation (Gilbert et al., 2007).

It has been hypothesized that some cellular mRNAs exhibit a relaxed cap dependence because of the presence of so-called cap-independent translation enhancers (CITEs) within the untranslated region (Terenin et al., 2013). CITEs are elements in the mRNA capable of recruiting key initiation factors, thereby promoting the assembly of translation initiation complexes. Despite years of speculation, the nature of CITE elements remains obscure. We recently discovered that mRNA methylation in the form of m^{6}A enables cap-independent translation (Meyer et al., 2015; Zhou et al., 2015). As exemplified by selective translation of heat shock-induced Hsp70 mRNA, this finding suggests the existence of a translation initiation mechanism that is neither cap nor IRES dependent. This new mode of translation initiation offers an attractive solution to the central puzzle that many

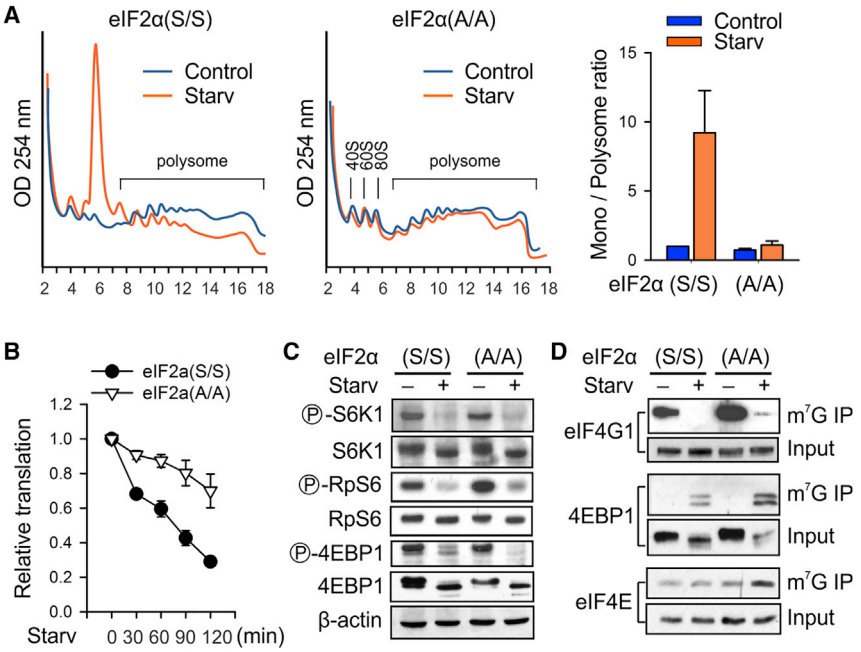

Figure 1. A Substantial Amount of Cellular Translation Is Resistant to eIF4F Inhibition

(A) Sucrose gradient-based polysome profiling of eIF2α (S/S) and eIF2α (A/A) MEF cells before and after 1 hr of amino acid starvation. The right panel shows the monosome/polysome ratio calculated using areas below the curve. Error bars, mean ± SEM; n = 3, biological replicates.

(B) Global protein synthesis in starved eIF2α(S/S) and eIF2α(A/A) MEF cells was quantified from puromycin labeling. Error bars, mean ± SEM; n = 3, biological replicates.

(C) Immunoblotting of mTORC1 downstream targets in eIF2α(S/S) and eIF2α(A/A) MEF cells before and after 1 hr of amino acid starvation.

(D) Immunoblotting of m^{7}GTP pulldown assay in eIF2α(S/S) and eIF2α(A/A) MEF cells before and after 1 hr of amino acid starvation.

See also Figures S1–S3.

cap-independent translation events do not follow the IRES mechanism. However, mechanistic details underlying m^{6}A-mediated translation initiation are poorly understood. Several fundamental questions remain unanswered. First, since many transcripts bear 5′ UTR methylation, how much does m^{6}A-mediated translation contribute to cellular protein synthesis? Second, for capped mRNAs with 5′ UTR methylation, are the canonical cap-dependent translation and the m^{6}A-enabled cap-independent translation mutually exclusive? Third, what is the biological logic behind the selection for different modes of translation initiation? Here, we investigated the scope and mechanism of eIF4F-independent mRNA translation, which revealed a dynamic coordination between different translation modes in response to environmental and physiological stimuli.

RESULTS

The Scope of Physiological Cap-Independent Translation

In response to amino acid deprivation, global protein synthesis is suppressed via inhibition of mTORC1 and activation of the general control non-derepressible-2 kinase (GCN2) (Hinnebusch, 2005; Ma and Blenis, 2009; Wek et al., 2006; Zoncu et al., 2011). While the former regulates eIF4F-mediated 5′ end cap recognition, the latter controls the formation of a ternary complex (TC) comprised of eIF2, GTP, and methionine-loaded initiator tRNA (Pisarev et al., 2007). To dissect the contribution of these two rate-limiting steps to the overall translational output, we took advantage of a mouse embryonic fibroblast (MEF) cell line harboring a non-phosphorylatable eIF2α in which the serine 51 (S/S) was mutated to an alanine (A/A) (Scheuner et al., 2001). As expected, wild-type eIF2α (S/S) cells readily responded to amino acid deprivation by showing polysome disassembly and concomitant increase of monosome (Figure 1A). To our surprise, eIF2α (A/A) cells showed few changes in the polysome pattern upon amino acid starvation. Consistently, measurement of global protein synthesis revealed much less repression of translation in starved eIF2α (A/A) cells than the wild-type (Figure 1B; Figure S1A). The striking resistance to amino acid limitation is also seen in cells lacking GCN2 kinase (Figure S1B). In addition, this phenomenon is highly reproducible under different types of stress, such as unfolded protein response in the endoplasmic reticulum (Figure S1C).

Amino acid deprivation is expected to inhibit mTORC1 signaling and consequently suppress eIF4F complex formation at the 5′ end cap (Jewell et al., 2013). It is thus surprising to observe continuous translation in starved eIF2α (A/A) cells. Previous studies suggested that the sensitivity of mTORC1 to nutrient starvation is coupled with GCN2/eIF2α signaling (Ye et al., 2015). It is possible that, in the absence of eIF2α phosphorylation, mTORC1 remains active even under limited supply of amino acids. However, this is not the case. Similar to wild-type cells, eIF2α (A/A) cells exhibited rapid dephosphorylation of mTORC1 downstream targets S6K1 and 4E-BP1 upon amino acid deprivation (Figure 1C). Notably, the phosphorylation status of the elongation factor eEF2 was comparable between S/S and A/A cells (Figure S1D). To directly measure the cap functionality in these cells, we conducted a m^{7}G cap pull-down assay before and after nutrient starvation. It is clear that, upon amino acid deprivation, the m^{7}G-associated scaffold protein eIF4G1 was largely replaced by 4E-BP1 in both wild-type and eIF2α (A/A) cells (Figure 1D). Therefore, the cap-recognition machinery is inactive under amino acid starvation irrespective of eIF2α phosphorylation.

To independently assess the contribution of cap recognition to global protein synthesis, we took advantage of a chemical compound 4EGI-1 that inhibits eIF4F complex formation by destabilizing eIF4E-eIF4G interaction (Moerke et al., 2007). [^{35}S] metabolic labeling revealed approximately 30% reduction in protein synthesis in both eIF2α (S/S) and (A/A) cells (Figure S2A). Notably, the majority of cellular translation sustained even after

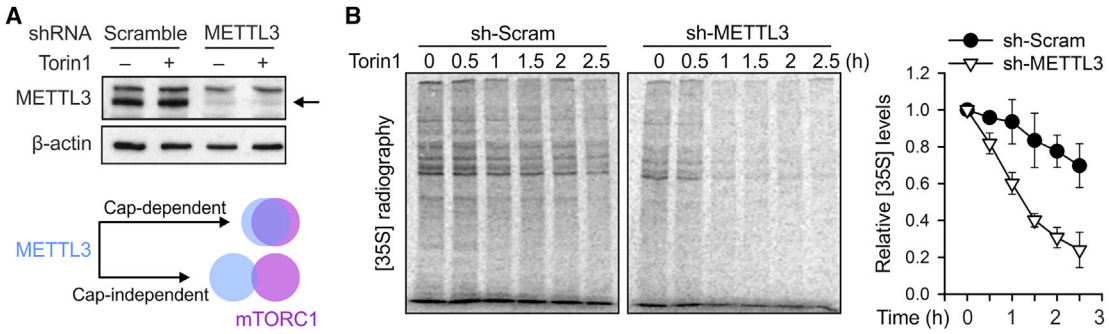

Figure 2. Physiological Cap-Independent Translation Is Dependent on m^{6}A Modification

(A) Immunoblotting of MEFs with or without METTL3 knockdown. The lower panel shows a schematic diagram distinguishing cap-dependent and cap-independent translation.

(B) Global protein synthesis in MEF cells with or without METTL3 knockdown was measured after pre-treatment of 1 μM Torin1 for various times. The right panel shows quantification of [^{35}S] autoradiograph after Torin1 treatment. Error bars, mean ± SEM; n = 3, biological replicates.

See also Figure S4.

prolonged treatment of 4EGI-1 (5 hr). We next examined the effect of Torin1, a potent active-site mTOR inhibitor (Thoreen et al., 2009). As expected, Torin1 treatment caused a rapid depletion of phosphorylation for mTORC1 downstream targets (Figure S2B). However, pre-exposure of cells to a high dose of Torin1 (1 μM) only led to less than 50% reduction in protein synthesis (Figure S2C). Therefore, a substantial amount of translation likely follows a mechanism independent of eIF4F.

Cap-Independent Translation Follows a Non-IRES Mechanism

It is possible that the translation maintained under eIF4F inactivation relies on a cap-independent mechanism like IRES or, as recently reported, an alternative cap-recognition mechanism mediated by eIF3d (Lee et al., 2016). In both cases, only a small subset of mRNAs undergo specialized translation. However, we found similar patterns of translational products resolved on the SDS-PAGE gel before and after eIF4F inactivation (Figures S1 and S2). This result suggests that the same transcripts are capable of experiencing different modes of translation. We next examined the sensitivity of eIF4F-independent translation to hippuristanol, an eIF4A inhibitor that does not affect certain IRES-driven translation (Bordeleau et al., 2006). Nearly all of the translations were repressed in the presence of hippuristanol irrespective of eIF2α signaling (Figure S3A). Therefore, eIF4F-independent translation still requires the scanning process. Further supporting its non-IRES feature, we observed minimal activation of IRES-driven translation in starved eIF2α(A/A) cells (Figure S3B). These results collectively suggest that, when the eIF4F-dependent translation is inactivated, cells readily employ a different mode of translation that is neither cap nor IRES dependent.

m^{6}A Mediates Translation That Is Neither Cap Nor IRES Dependent

We previously reported that m^{6}A enables mRNA translation in a cap- and IRES-independent manner (Meyer et al., 2015; Zhou et al., 2015). We next investigated whether the substantial amount of translation persisted under eIF4F inactivation follows the m^{6}A-dependent mechanism. To test this possibility, we knocked down METTL3, a core subunit of methyltransferase complex, from MEF cells using shRNA. With more than 90% depletion of METTL3 (Figure 2A), we observed approximately 50% reduction of m^{6}A levels on mRNAs (Figure S4A). METTL3 knockdown caused nearly 30% decrease of global protein synthesis (Figure S4B), which is consistent with the recent study that reported cytosolic function of METTL3 in translation (Lin et al., 2016). However, it is unresolved whether METTL3 plays a role in cap-dependent or cap-independent translation. We reasoned that if METTL3 mediates cap-dependent translation, the translational targets sensitive to METTL3 knockdown should overlap with mTORC1-sensitive targets. If so, METTL3 depletion is not expected to further decrease protein synthesis in the presence of mTORC1 inhibitors. In stark contrast, MEFs lacking METTL3 exhibited much greater sensitivity to Torin1 than the scramble control (Figure 2B), with nearly 80% reduction of protein synthesis after 2 hr treatment of Torin1. To substantiate this finding further, we conducted METTL14 knockdown in MEF cells. Similar to METTL3 depletion, reducing METTL14 also sensitized MEF cells to Torin1 treatment (Figure S4C). The additive effect between methyltransferase knockdown and Torin1 treatment clearly indicates that m^{6}A-responsible mRNA translation differs from eIF4F-controlled protein synthesis. To ensure that it is the m^{6}A modification rather than the physical METTL3 binding that mediates eIF4F-independent translation, we complemented with either wild-type METTL3 or an inactive D395A mutant to MEFs lacking endogenous METTL3. In the presence of Torin1, only the wild-type METTL3, but not the mutant, restored the global protein synthesis (Figure S4D).

m^{6}A-Mediated Translation Differs from eIF4F in mRNA Targets

To elucidate the scope of m^{6}A-mediated translation, we examined the translation potential of endogenous transcripts in cells with either METTL3 knockdown or eIF4F inhibition. Previous genome-wide studies revealed that the mRNA subsets highly sensitive to mTORC1 signaling consist almost entirely of transcripts with 5′ terminal oligopyrimidine (TOP) elements

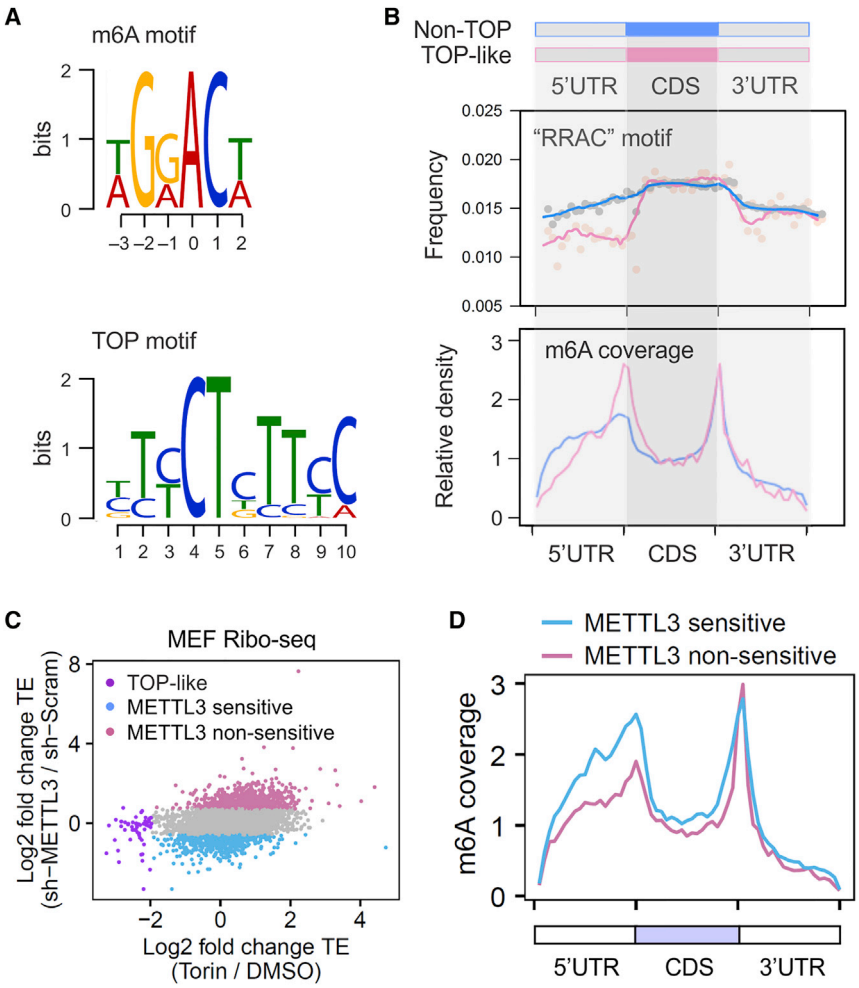

Figure 3. m^{6}A Mediates eIF4F-Independent Translation

(A) Sequence logo representing the consensus motif relative to m^{6}A (top) and TOP elements (bottom, derived from Thoreen et al., 2012). For m^{6}A motif, "0" indicates the position of m^{6}A. For TOP motif, "1" represents the 5′ end position.

(B) The top panel shows the frequency of m^{6}A motif across TOP-like (pink line) and non-TOP (blue line) mRNAs. The lower panel shows the distribution of m^{6}A modification across TOP-like (pink line) and non-TOP (blue line) mRNAs using m^{6}A-seq datasets obtained from MEFs.

(C) Scatterplot shows the TE fold change in MEF cells in response to Torin1 treatment or METTL3 knockdown. Blue dots refer to TOP-like transcripts. Both METTL3-sensitive (bottom 10%) and non-sensitive (top 10%) mRNAs are highlighted.

(D) m^{6}A coverage obtained from m^{6}A-seq was plotted for METTL3 non-sensitive (pink line) and METTL3 sensitive (blue line) mRNAs. Relative regions of 5′ UTR, CDS, and 3′ UTR are shown as the same size.

See also Figure S4.

(Hsieh et al., 2012; Thoreen et al., 2012). Supporting this notion, the translation of these TOP mRNAs was highly sensitive to Torin1 treatment as revealed by ribosome profiling (Ribo-seq) in MEF cells (Figure S4E). Given the mutually exclusive nature between the TOP motif and m^{6}A sequence context (Figure 3A), it is possible that TOP mRNAs in general have less m^{6}A modification in the 5′ UTR and thus heavily rely on the cap-dependent mechanism for translation. Indeed, sequence survey of mouse transcriptome revealed low levels of m^{6}A consensus sequence in the 5′ UTR of TOP mRNAs (Figure 3B). We further compared the methylation landscape between TOP and non-TOP mRNAs using m^{6}A-seq data derived from MEF cells (Geula et al., 2015). Virtually no m^{6}A modification occurs at the first half of TOP 5′ UTR. Since both coding region sequence (CDS) and 3′ UTR regions show comparable m^{6}A distribution between TOP and non-TOP mRNAs, we argue that it is the 5′ UTR sequence feature that influences the relative cap dependency during translation.

To test this hypothesis, we examined ribosome profiling datasets obtained from MEF cells depleted of METTL3. Indeed, TOP mRNAs showed little response to METTL3 knockdown (*Rho* = 0.11) (Figure 3C). In coupling with m^{6}A-seq datasets, we found that transcripts undergoing translational downregulation in the absence of METTL3 generally had higher 5′ UTR methylation levels (Figure 3D). The similar observation was evident when we used different m^{6}A-seq datasets derived from MEF cells (Schwartz et al., 2014) (Figure S4F). As an independent validation, we analyzed datasets obtained from HeLa cells with or without METTL3 depletion (Wang et al., 2015). Direct comparison of the translation efficiency (TE) revealed that translation of non-TOP mRNAs was more sensitive to METTL3 depletion than that of TOP mRNAs ($p = 2.2 \times 10^{-16}$) (Figure S4G). Taken together, these data suggest that m^{6}A modification in the 5′ UTR renders these transcripts insensitive to eIF4F inhibition by enabling cap-independent translation.

To search for potential m^{6}A readers that mediate eIF4F-independent mRNA translation, we examined YTH domain family proteins residing in the cytoplasm. Interestingly, knocking down YTHDF3, but not YTHDF1 and YTHDF2, re-sensitized MEF cells to Torin1 treatment (Figure S5A). The putative role of YTHDF3 in eIF4F-independent translation is consistent with several recent studies reporting that YTHDF3 facilitated mRNA translation, including m^{6}A-mediated circular RNA translation (Li et al., 2017; Shi et al., 2017; Yang et al., 2017).

METTL3 Recognizes Internal m^{6}A, but Not the m^{7}G Cap

Previous studies demonstrated that exogenously overexpressed METTL3 co-immunoprecipitated with cap-binding proteins such as CBP80/20 and eIF4E (Lin et al., 2016). These results have been interpreted as fitting a model in which METTL3 promotes cap-dependent translation. To test the cap-binding capability

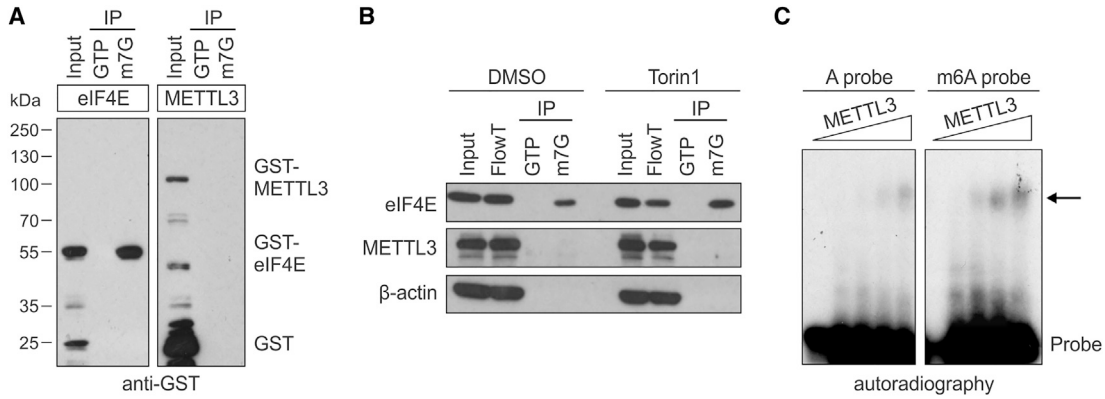

Figure 4. METTL3 Recognizes m^{6}A, but Not the m^{7}G, Cap Structure

(A) Recombinant eIF4E and METTL3 proteins were purified from *E. coli* as GST fusion proteins followed by incubation with immobilized beads coated with m^{7}GTP. Immunoblotting was conducted using an anti-GST antibody.

(B) Whole-cell lysates from HEK293 cells with or without Torin1 treatment were incubated with immobilized beads coated with m^{7}GTP followed by immunoblotting using antibodies indicated.

(C) Synthesized mRNA probes with or without single m^{6}A were radiolabeled with ^{32}P followed by incubation with an increasing dose of recombinant METTL3 (0, 0.3, 0.6, 1.2, and 2.4 μg). The mRNA-protein complexes were resolved on a SDS-PAGE gel.

See also Figure S5.

of METTL3, we employed a direct cap-binding assay using recombinant proteins purified from *E. coli*. The immobilized m^{7}G cap readily precipitated eIF4E, as expected, but failed to pull down METTL3 (Figure 4A). We next examined the cap-binding feature of endogenous proteins by incubating the m^{7}G beads with whole-cell lysates. Although the m^{7}G cap readily pull down a considerable amount of eIF4E, no detectable METTL3 was precipitated by the m^{7}G cap (Figure 4B). Notably, the m^{7}G cap failed to capture METTL3 upon mTORC1 inhibition, despite the fact that more eIF4E molecules were recovered from the same lysates. Therefore, endogenous METTL3 does not bind to the cap structure regardless of the functional status of eIF4F.

Given the inherent AdoMet binding pocket of METTL3 (Wang et al., 2016a; Wang et al., 2016b), we next examined whether METTL3 directly interacts with methylated mRNA. Using a synthesized 30 nt mRNA with or without a single m^{6}A site at the consensus sequence, we conducted a gel-shifting assay. Although the non-methylated probe weakly associated with METTL3, introducing a single m^{6}A site significantly promoted METTL3 binding (Figure 4C). By contrast, METTL3 showed little preference in association with the capped mRNA synthesized via *in vitro* transcription (Figure S5B). This result indicates that METTL3 directly binds to the internal m^{6}A, but not the 5′ end cap structure.

Cap-Independent Translation of Hsp70 Requires ABCF1

We previously demonstrated that m^{6}A enables cap-independent translation, especially under stress conditions. However, it is unclear how 5′ UTR methylation promotes preinitiation complex assembly without forming the canonical eIF4F complex. In an attempt to identify potential mediators responsible for m^{6}A-mediated cap-independent translation, we employed quantitative proteomic analysis to compare proteins associated with the same message experiencing cap-dependent or cap-independent translation. Hsp70 mRNA undergoes translational switch in response to heat shock stress (Zhou et al., 2015) and represents an ideal endogenous transcript to address this question. We adopted a method based on endogenous mRNA pull-down without chemical crosslinking using biotinylated probes (Figure 5A). To identify and quantify the associated protein components, we employed an unbiased quantitative approach where digested peptides were labeled with 4-plex isobaric mass tags (iTRAQ) and subjected to liquid chromatography-tandem mass spectrometry analysis (LS-MS/MS). In addition to Hsp70 mRNA, we included β-actin mRNA as a control. HeLa was chosen because of the relatively high basal level of Hsp70 mRNA prior to heat shock stress, therefore permitting direct comparison of components associated with the same transcript before and after stress.

As expected, nearly all the ribosomal proteins showed reduced enrichment after heat shock stress, forming a distinct cluster with high peptide scores (Figure 5A; Table S1). Interestingly, several translation initiation factors were selectively enriched on the Hsp70 transcript, but not the β-actin mRNA, upon heat shock stress (Figure 5A, right). Among the most prominent factors are α, β, and γ subunits of eIF2 (>9-fold). Since eIF2 controls the ternary complex formation, it is clear that the stress-induced Hsp70 mRNA is capable of recruiting the initiator tRNA even when the cap recognition machinery is inactive under heat shock stress. A close inspection of the quantitative proteomic data revealed that eIF2A, eIF5, and ABCF1 were also associated with the stress-induced Hsp70 mRNA. In particular, ABCF1 showed a similar stoichiometry as eIF2 as judged by their comparable peptide scores (Figure 5A, right).

We validated the proteomic result by conducting immunoprecipitation (IP) of various endogenous proteins from cell lysates before and after stress. The non-canonical initiation factor eIF2A failed to pull down typical initiation factors such as eIF4G1 and eIF2β (Figure 5B). By contrast, eIF5 constitutively associated with these initiation factors irrespective of the stress

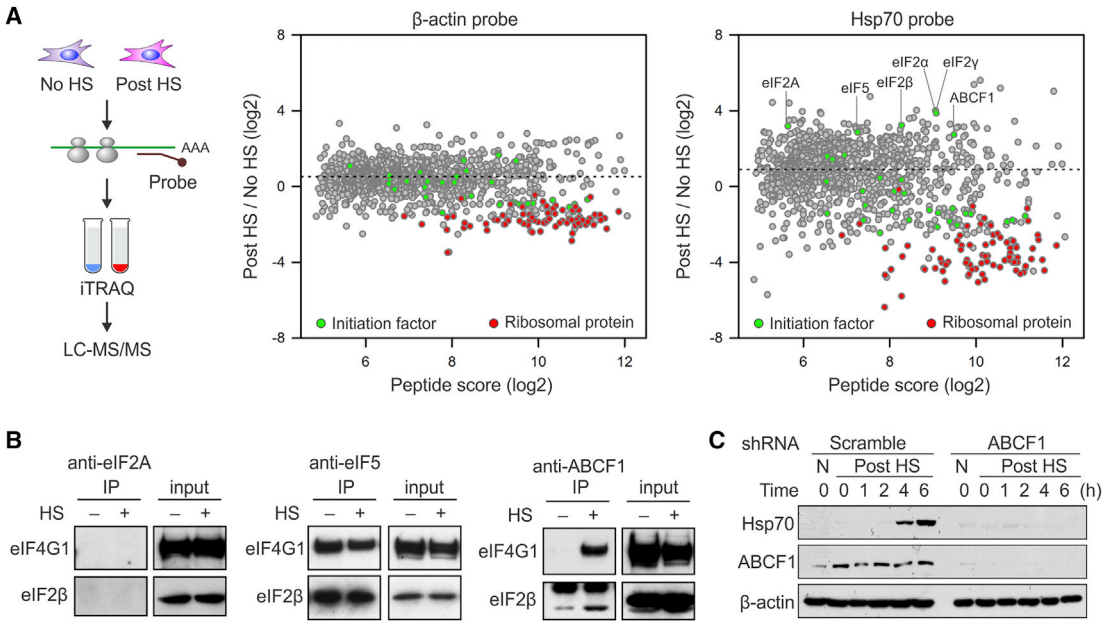

Figure 5. ABCF1 Is Essential in Cap-Independent Translation of Hsp70

(A) The left panel shows the schematic of quantitative mass spectrometry using iTRAQ. Proteins enriched on β-actin mRNA (middle) or Hsp70 mRNA (right) purified from HeLa cells after heat shock stress are presented as scatterplots. The original peptide score (log_2) and stress-induced fold changes (log_2) are shown in the x axis and the y axis, respectively.

(B) Whole-cell lysates from heat-shocked HeLa cells were subjected to immunoprecipitation using antibodies indicated followed by immunoblotting.

(C) MEF cells with or without ABCF1 knockdown (Scramble) were collected at indicated times after heat shock stress (43°C, 1 hr) followed by immunoblotting. N, no heat shock.

See also Figure S6.

condition. Only ABCF1 was able to precipitate eIF4G1 and eIF2β in a stress-dependent manner (Figure 5B). These results suggest that ABCF1 facilitates initiation complex assembly on stress messages in response to heat shock stress. To resolve the physiological role of ABCF1 in stress-induced Hsp70 synthesis, we knocked down ABCF1 in MEF cells using shRNA-expressing lentiviruses. Remarkably, after heat shock stress, the Hsp70 synthesis was severely abolished in cells lacking ABCF1 (Figure 5C). The critical role of ABCF1 in Hsp70 synthesis was also seen in HeLa cells, despite the different basal levels of these proteins (Figures S6A and S6B). Notably, the cellular Hsp70 mRNA levels were even higher in cells with ABCF1 knockdown (Figure S6C), further supporting the translational deficiency of Hsp70 synthesis in the absence of ABCF1.

ABCF1 Facilitates m^{6}A-Mediated Translation

Having found that a substantial amount of cellular translation follows the eIF4F-independent mechanism under the normal growth condition, we asked whether ABCF1 is also responsible for physiological cap-independent translation. ABCF1 knockdown in non-stressed MEFs resulted in about 20% reduction of global protein synthesis (Figure S6D), which is consistent with the previous report (Paytubi et al., 2009). To confirm that ABCF1-responsible translation indeed follows cap-independent initiation mode, we suppressed eIF4F-dependent translation by Torin1 treatment. Similar to the cells lacking METTL3, ABCF1 knockdown rendered MEF cells highly sensitive to Torin1 treatment by showing >80% reduction of protein synthesis (Figure 6A). The increased sensitivity to mTOR1 inhibition in the absence of ABCF1 supports the notion that ABCF1-responsible translation differs from eIF4F-mediated cap-dependent translation.

Since ABCF1 resembles METTL3 in mediating eIF4F-independent translation, we predicted that the ABCF1-sensitive transcripts should overlap with METTL3-responsible mRNA targets. This is indeed the case. Ribosome profiling of MEF cells lacking either ABCF1 or METTL3 showed a strong correlation in the changes of TE ($r = 0.57$; Figure 6B). Further supporting the notion that ABCF1 facilitates m^{6}A-mediated translation, transcripts experiencing decreased translation in the absence of ABCF1 have higher 5′ UTR methylation than the one resistant to ABCF1 depletion (Figure 6C). Taken together with the crucial role of ABCF1 and METTL3 in the cap-independent translation of Hsp70 (Figure S6E), these results indicate a functional coordination between ABCF1 and METTL3 in m^{6}A-facilitated translation.

ABCF1 Controls METTL3 Translation

ABCF1 (also termed ABC50) is an ATP-binding cassette protein that, unlike most ABC proteins, lacks membrane-spanning domains (Paytubi et al., 2009; Tyzack et al., 2000). Previous studies demonstrated that ABCF1 promotes translation initiation by interacting with eIF2 and ribosomes (Paytubi et al., 2009; Tyzack et al., 2000). Curiously, in MEF cells lacking

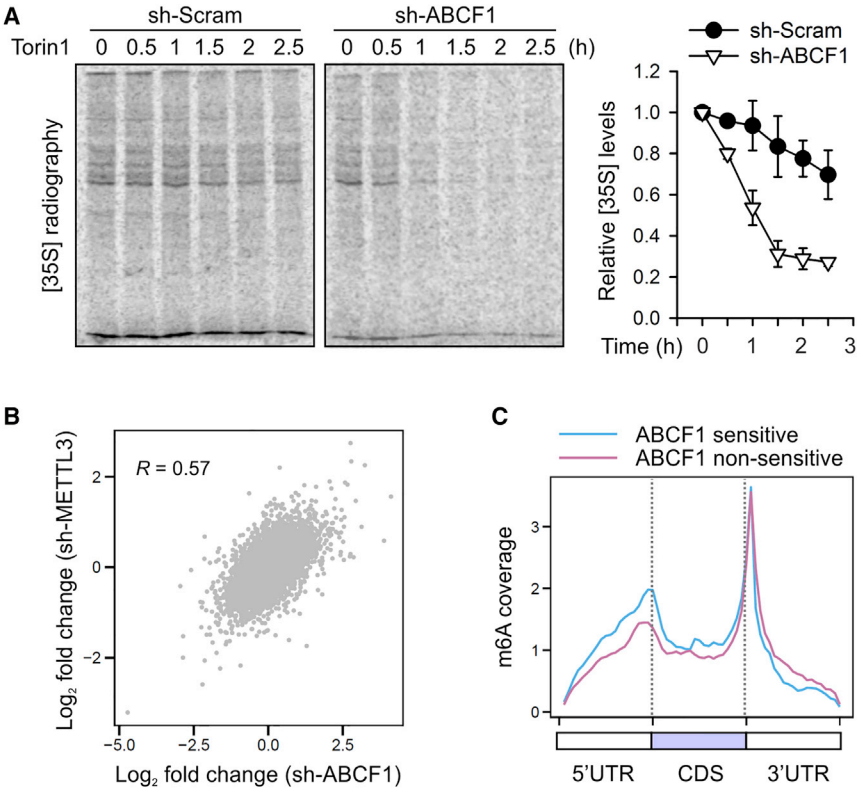

Figure 6. ABCF1 Mediates eIF4F-Independent Translation

(A) Global protein synthesis in MEF cells with or without ABCF1 knockdown was measured after pre-treatment of 1 μM Torin1 for various times. The right panel shows quantification of [^{35}S] autoradiograph after Torin1 treatment. Error bars, mean ± SEM; n = 3, biological replicates.

(B) Ribosome profiling data from cells with ABCF1 or METTL3 knockdown were used to determine the fold changes of TE. A scatterplot is presented to show positive correlation.

(C) m^{6}A coverage obtained from m^{6}A-seq was plotted for ABCF1-sensitive (blue line) and non-responsive (pink line) mRNAs. Relative regions of 5′ UTR, CDS, and 3′ UTR are shown as the same size.

See also Figure S6.

ABCF1, there was a decreased steady-state level of endogenous METTL3 (Figure 7A). In METTL3-depleted cells, however, the level of ABCF1 was not affected. The reduced METTL3 in the absence of ABCF1 was not due to altered mRNA levels as qPCR revealed little changes of *Mettl3* in cells lacking ABCF1 (Figure 7B). This unexpected finding is reminiscent of reduced METTL3 stability in cells lacking METTL14 (Liu et al., 2014), suggesting that ABCF1 could serve as a binding partner for METTL3. However, proteasome inhibition by MG132 treatment did not restore the level of METTL3 (Figure 7A). In addition, we failed to detect the mutual interaction between METTL3 and ABCF1 from either endogenous proteins or transfected genes bearing affinity tags (Figures S7A and S7B). This result is nevertheless consistent with the distinct cellular localization of these proteins: while METTL3 is predominantly a nuclear protein, ABCF1 is mainly localized in the cytoplasm (Figure S7C).

Given the critical role of ABCF1 in mRNA translation under stress, we asked whether ABCF1 controls the translation of METTL3. Interestingly, m^{6}A-seq datasets from human cells revealed that the METTL3 mRNA is heavily methylated in the 5′ UTR, but not 3′ UTR (Figure 7C). This unique feature is suggestive of relaxed cap dependency in METTL3 translation. To test this possibility, we constructed a reporter by placing the 5′ UTR of *Mettl3* before the firefly luciferase (Fluc) coding region. While the Fluc control showed about 50% reduction of translation in the presence of Torin1, *Mettl3*-Fluc showed little response to mTOR inhibition (Figure 7D). However, depleting ABCF1 significantly decreased METTL3-Fluc translation (Figure 7D, right). The m^{6}A-facilitated translation of m^{6}A "writer" METTL3 suggests a self-regulatory mechanism that offers an alternative translation mode when the cap machinery is inhibited.

DISCUSSION

For years, researchers have been fixated on the idea that eukaryotic mRNA translation relies on two mutually exclusive mechanisms: cap-dependent ribosome scanning and cap-independent internal ribosome entry. Despite the predominant belief that eIF4F-mediated cap-dependent translation contributes to the majority of protein synthesis in eukaryotic cells, it is puzzling that inhibiting cap recognition by chemical inhibitors or genetic ablation only has modest effect on protein synthesis (Beretta et al., 1996; Choo et al., 2008; Yanagiya et al., 2012). The simplest interpretation of this conundrum is that cells rely on cap-independent initiation mechanism for a substantial amount of mRNA translation. The IRES-driven translation has become essentially synonymous with 5′ cap-independent mRNA translation. However, the extent of cellular mRNAs that have been considered to contain IRESs remains controversial (Gilbert, 2010). Although certain mRNAs use the IRES mechanism to achieve the ribosome specificity (Xue et al., 2015), additional concepts are needed to explain how cells maintain robust translation during episodes of eIF4F inhibition. Here, we report that m^{6}A-mediated translation initiation follows a cap- and IRES-independent mechanism. Unlike IRES-driven or eIF3d-mediated specialized translation, the m^{6}A-promoted translation co-exists with eIF4F-mediated translation initiation for a great deal of transcripts. The scope of cap-independent translation is therefore much broader than previously appreciated.

METTL3 is an essential enzyme for m^{6}A modification of mRNAs, which primarily occurs in the nucleus (Liu et al., 2014). A recent study adds a new twist to its functionality by demonstrating a cytosolic role of METTL3 in translation (Lin et al., 2016). It surprisingly acts as a "reader" rather than a "writer" of methylated transcripts because the m^{6}A catalytic activity

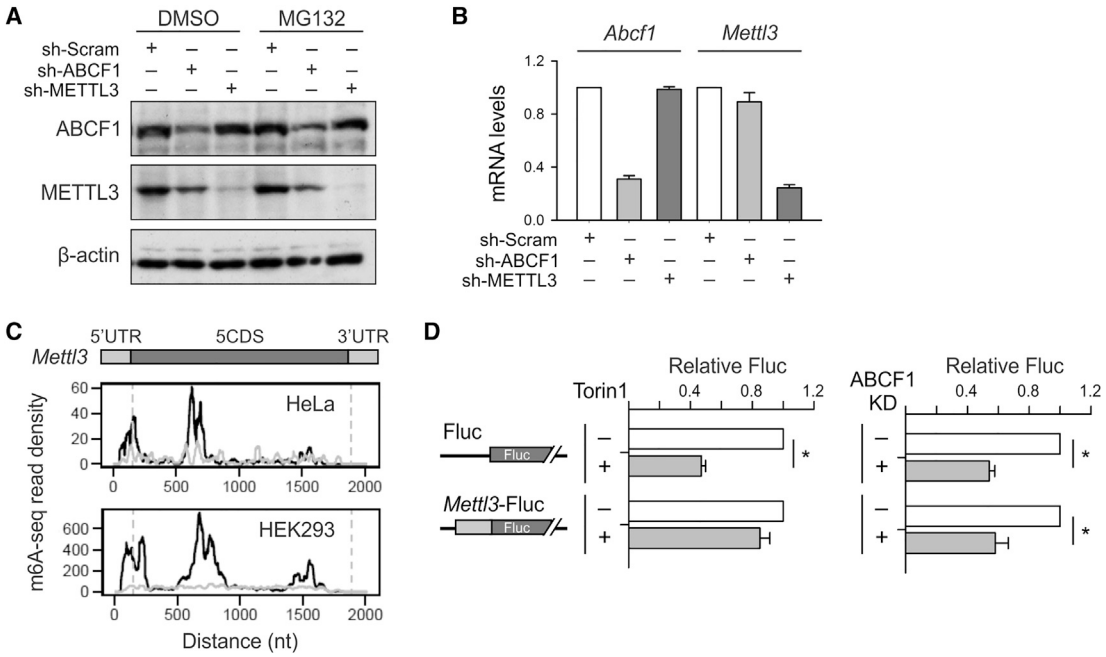

Figure 7. ABCF1 Mediates Translational Control of METTL3

(A) MEF cells with ABCF1 or METTL3 knockdown were treated with 5 μM MG132 for 16 hr. Whole-cell lysates were collected for immunoblotting using the antibodies indicated.

(B) Total RNAs were purified from MEF cells with ABCF1 or METTL3 knockdown followed by qPCR. Error bars, mean ± SEM; n = 3, biological replicates.

(C) m^{6}A coverage of METTL3 mRNA using m^{6}A-seq datasets obtained from HeLa and HEK293 cells. The transcript architecture is shown above.

(D) MEF cells were transfected with Fluc plasmids shown in the left and Fluc levels were recorded by real-time luminometry. Error bars, mean ± SEM; n = 3, biological replicates. *p < 0.05 (t test).

See also Figure S7.

is dispensable in METTL3-promoted translation (Lin et al., 2016). However, it is unclear why only a subset of mRNAs is subjected to translational regulation by METTL3 in this manner. Although METTL3 appears to promote translation in cancer cells, it is not essential in embryonic stem cells (Geula et al., 2015). These puzzling observations call into question the exact role of METTL3 in translational regulation. One of the key questions is whether METTL3-promoted translation follows cap-dependent or cap-independent mechanisms. We provided evidence that METTL3, in fact, primarily facilitates translation independent of eIF4F. In addition, METTL3 does not seem to have the m^{7}G cap-binding capacity, although it readily associates with internal m^{6}A sites. The finding that m^{6}A-mediated translation occurs on fully capped mRNAs suggests that the same transcript undergoes multiple translational modes, which explains the incomplete inhibition of translation by eIF4F inactivation. Indeed, only under the inactivation of mTORC1 signaling does the remaining translation become highly sensitive to METTL3 depletion. Intriguingly, a recent study reported that m^{6}Am at the 5′ end of mRNAs stabilizes mRNAs and likely promotes translation (Mauer et al., 2017). Since m^{6}Am is part of the 5′ cap structure, it is of importance to demonstrate whether m^{6}Am functions as internal m^{6}A or coordinates with the m^{7}G cap in translational control.

What advantage might m^{6}A-mediated translation confer when the cap machinery is fully functional inside cells? The answer to this question has two distinct, but interwoven, parts. The first lies in the selectivity of mRNA translation and the second lies in the redistribution of cellular resources. Although mTORC1 primarily controls cap-dependent mRNA translation, it preferentially regulates the translation of TOP mRNAs via poorly understood mechanisms (Hamilton et al., 2006; Thoreen et al., 2012). Notably, the TOP mRNAs are among the most abundant messages in the cell, comprising up to 30% of cellular mRNAs during rapid growth in rich media (Warner, 1999). It is not surprising that the translation of TOP mRNAs must be quickly attenuated in response to limited supply of amino acids. It is conceivable that a diverse group of mRNAs must maintain their translation irrespective of the nutrient signaling. The m^{6}A-mediated translation permits translation of some "privileged" mRNAs to produce proteins important for cell maintenance as well as cell survival. We propose that different modes of translation are coordinated to produce adaptive translatomes in response to environmental and physiological stimuli.

Under stress conditions, like amino acid starvation, the amount of ternary complex becomes limited as a result of GCN2-triggered eIF2α phosphorylation (Liu and Qian, 2014; Wek et al., 2006). How does m^{6}A-mediated translation initiation acquire the ternary complex to ensure productive translation? We found that ABCF1 serves as an alternative recruiter for the ternary complex during non-canonical translation. ABCF1 is a close relative of the yeast protein GCN20, which is presumed to cooperate with GCN1 in starvation-induced translational

response (Marton et al., 1997). Although GCN20 and ABCF1 are similar in their ABC domains, they differ markedly in their N termini. Intriguingly, it is the N-terminal region of ABCF1 that interacts with eIF2 in mammalian cells (Paytubi et al., 2008). In cells lacking ABCF1, heat shock-induced Hsp70 translation was severely impaired. Importantly, ABCF1 also plays a role in m^6A-facilitated translation under the normal growth condition. Not surprisingly, cells with ABCF1 knockdown exhibits similar translational phenotypes as cells lacking METTL3. Perhaps the most interesting finding is the self-regulation of METTL3 translation that is not only dependent on m^6A, but also subjected to ABCF1 regulation. This positive feedback loop provides a mechanism by which cells activate m^6A-mediated translation upon inhibition of cap-dependent translation. Since the cap machinery evolved at a late stage during eukaryogenesis after the emergence of the nucleus and mRNA cap structure (Hernández, 2009), it is conceivable that a cap-independent initiation mechanism exists for capped mRNAs in early eukaryotes. The dynamic coordination between different translation modes encourages us to reconsider our traditional view of eIF4F as the primary driver of protein synthesis.

STAR★METHODS

Detailed methods are provided in the online version of this paper and include the following:

- KEY RESOURCES TABLE
- CONTACT FOR REAGENT AND RESOURCE SHARING
- EXPERIMENTAL MODEL AND SUBJECT DETAILS
  - Cell Lines and Reagents
  - Lentiviral shRNAs
- METHOD DETAILS
  - Puromycin Labeling
  - [^{35}S] Radiolabeling
  - Cap Pull-Down
  - Immunoblotting
  - mRNA Pull-Down Using DNA Probes
  - Mass Spectrometry
  - Real-Time PCR
  - *In Vitro* Transcription
  - Real-Time Luciferase Assay
  - Electrophoretic Mobility Shift Assay
  - Recombinant Protein Purification and *In Vitro* Cap-Binding Assay
  - Immunofluorescence Staining
  - Co-immunoprecipitation Assay
  - m^6A Dot Blot
  - Polysome Profiling Analysis
  - RNA-Seq and m^6A-Seq
  - Ribo-Seq
  - cDNA Library Construction
  - Deep Sequencing
- QUANTIFICATION AND STATISTICAL ANALYSIS
  - Preprocessing of Sequencing Reads
  - Identification of m^6A Sites
  - Motif Analysis
- DATA AND SOFTWARE AVAILABILITY

SUPPLEMENTAL INFORMATION

Supplemental Information includes seven figures and one table and can be found with this article online at https://doi.org/10.1016/j.molcel.2017.10.002.

AUTHOR CONTRIBUTIONS

R.A.C. and S.-B.Q. conceived the project and designed the study. R.A.C. performed most of the experiments. X.-M.L. performed cap binding and protein interaction assays as well as Ribo-seq and RNA-seq. Y.M. and J.W. analyzed the sequencing data. J.Z. conducted m^6A-seq. L.D. assisted Ribo-seq. X.Z. conducted MS experiment. S.-B.Q. wrote the manuscript. All authors discussed results and edited the manuscript.

ACKNOWLEDGMENTS

We'd like to thank Dr. Jerry Pelletier for providing hippuristanol and Qian lab members for helpful discussion. We are grateful to Cornell University Life Sciences Core Laboratory Center for performing deep sequencing. This work was supported by grants to S.-B.Q. from US National Institutes of Health (R01AG042400), US Department of Defense (W81XWH-14-1-0068), and HHMI Faculty Scholar (55108556).

Received: February 13, 2017
Revised: July 25, 2017
Accepted: September 29, 2017
Published: October 26, 2017

REFERENCES

Alarcón, C.R., Goodarzi, H., Lee, H., Liu, X., Tavazoie, S., and Tavazoie, S.F. (2015). HNRNPA2B1 is a mediator of m(6)A-dependent nuclear RNA processing events. Cell *162*, 1299–1308.

Bailey, T.L., Boden, M., Buske, F.A., Frith, M., Grant, C.E., Clementi, L., Ren, J., Li, W.W., and Noble, W.S. (2009). MEME SUITE: tools for motif discovery and searching. Nucleic Acids Res. *37*, W202–W208.

Beretta, L., Gingras, A.C., Svitkin, Y.V., Hall, M.N., and Sonenberg, N. (1996). Rapamycin blocks the phosphorylation of 4E-BP1 and inhibits cap-dependent initiation of translation. EMBO J. *15*, 658–664.

Bordeleau, M.E., Mori, A., Oberer, M., Lindqvist, L., Chard, L.S., Higa, T., Belsham, G.J., Wagner, G., Tanaka, J., and Pelletier, J. (2006). Functional characterization of IRESes by an inhibitor of the RNA helicase eIF4A. Nat. Chem. Biol. *2*, 213–220.

Choo, A.Y., Yoon, S.O., Kim, S.G., Roux, P.P., and Blenis, J. (2008). Rapamycin differentially inhibits S6Ks and 4E-BP1 to mediate cell-type-specific repression of mRNA translation. Proc. Natl. Acad. Sci. USA *105*, 17414–17419.

Dominissini, D., Moshitch-Moshkovitz, S., Schwartz, S., Salmon-Divon, M., Ungar, L., Osenberg, S., Cesarkas, K., Jacob-Hirsch, J., Amariglio, N., Kupiec, M., et al. (2012). Topology of the human and mouse m6A RNA methylomes revealed by m6A-seq. Nature *485*, 201–206.

Gebauer, F., and Hentze, M.W. (2004). Molecular mechanisms of translational control. Nat. Rev. Mol. Cell Biol. *5*, 827–835.

Geula, S., Moshitch-Moshkovitz, S., Dominissini, D., Mansour, A.A., Kol, N., Salmon-Divon, M., Hershkovitz, V., Peer, E., Mor, N., Manor, Y.S., et al. (2015). Stem cells. m6A mRNA methylation facilitates resolution of naïve pluripotency toward differentiation. Science *347*, 1002–1006.

Gilbert, W.V. (2010). Alternative ways to think about cellular internal ribosome entry. J. Biol. Chem. *285*, 29033–29038.

Gilbert, W.V., Zhou, K., Butler, T.K., and Doudna, J.A. (2007). Cap-independent translation is required for starvation-induced differentiation in yeast. Science *317*, 1224–1227.

Gross, J.D., Moerke, N.J., von der Haar, T., Lugovskoy, A.A., Sachs, A.B., McCarthy, J.E., and Wagner, G. (2003). Ribosome loading onto the mRNA

cap is driven by conformational coupling between eIF4G and eIF4E. Cell *115*, 739–750.

Hamilton, T.L., Stoneley, M., Spriggs, K.A., and Bushell, M. (2006). TOPs and their regulation. Biochem. Soc. Trans. *34*, 12–16.

Hellen, C.U., and Sarnow, P. (2001). Internal ribosome entry sites in eukaryotic mRNA molecules. Genes Dev. *15*, 1593–1612.

Hernández, G. (2009). On the origin of the cap-dependent initiation of translation in eukaryotes. Trends Biochem. Sci. *34*, 166–175.

Hinnebusch, A.G. (2005). Translational regulation of GCN4 and the general amino acid control of yeast. Annu. Rev. Microbiol. *59*, 407–450.

Hinnebusch, A.G. (2014). The scanning mechanism of eukaryotic translation initiation. Annu. Rev. Biochem. *83*, 779–812.

Hsieh, A.C., Liu, Y., Edlind, M.P., Ingolia, N.T., Janes, M.R., Sher, A., Shi, E.Y., Stumpf, C.R., Christensen, C., Bonham, M.J., et al. (2012). The translational landscape of mTOR signalling steers cancer initiation and metastasis. Nature *485*, 55–61.

Jackson, R.J., Hellen, C.U., and Pestova, T.V. (2010). The mechanism of eukaryotic translation initiation and principles of its regulation. Nat. Rev. Mol. Cell Biol. *11*, 113–127.

Jewell, J.L., Russell, R.C., and Guan, K.L. (2013). Amino acid signalling upstream of mTOR. Nat. Rev. Mol. Cell Biol. *14*, 133–139.

Langmead, B., Trapnell, C., Pop, M., and Salzberg, S.L. (2009). Ultrafast and memory-efficient alignment of short DNA sequences to the human genome. Genome Biol. *10*, R25.

Lee, A.S., Kranzusch, P.J., Doudna, J.A., and Cate, J.H. (2016). eIF3d is an mRNA cap-binding protein that is required for specialized translation initiation. Nature *536*, 96–99.

Li, A., Chen, Y.S., Ping, X.L., Yang, X., Xiao, W., Yang, Y., Sun, H.Y., Zhu, Q., Baidya, P., Wang, X., et al. (2017). Cytoplasmic m(6)A reader YTHDF3 promotes mRNA translation. Cell Res. *27*, 444–447.

Lin, S., Choe, J., Du, P., Triboulet, R., and Gregory, R.I. (2016). The m(6)A methyltransferase METTL3 promotes translation in human cancer cells. Mol. Cell *62*, 335–345.

Liu, B., and Qian, S.B. (2014). Translational reprogramming in cellular stress response. Wiley Interdiscip. Rev. RNA *5*, 301–315.

Liu, J., Yue, Y., Han, D., Wang, X., Fu, Y., Zhang, L., Jia, G., Yu, M., Lu, Z., Deng, X., et al. (2014). A METTL3-METTL14 complex mediates mammalian nuclear RNA N6-adenosine methylation. Nat. Chem. Biol. *10*, 93–95.

Ma, X.M., and Blenis, J. (2009). Molecular mechanisms of mTOR-mediated translational control. Nat. Rev. Mol. Cell Biol. *10*, 307–318.

Marintchev, A., Edmonds, K.A., Marintcheva, B., Hendrickson, E., Oberer, M., Suzuki, C., Herdy, B., Sonenberg, N., and Wagner, G. (2009). Topology and regulation of the human eIF4A/4G/4H helicase complex in translation initiation. Cell *136*, 447–460.

Martin, M. (2011). Cutadapt removes adapter sequences from high-throughput sequencing reads. EMBnet J. *17*, 10–12.

Marton, M.J., Vazquez de Aldana, C.R., Qiu, H., Chakraburtty, K., and Hinnebusch, A.G. (1997). Evidence that GCN1 and GCN20, translational regulators of GCN4, function on elongating ribosomes in activation of eIF2alpha kinase GCN2. Mol. Cell. Biol. *17*, 4474–4489.

Mauer, J., Luo, X., Blanjoie, A., Jiao, X., Grozhik, A.V., Patil, D.P., Linder, B., Pickering, B.F., Vasseur, J.J., Chen, Q., et al. (2017). Reversible methylation of m(6)Am in the 5′ cap controls mRNA stability. Nature *541*, 371–375.

Meyer, K.D., Patil, D.P., Zhou, J., Zinoviev, A., Skabkin, M.A., Elemento, O., Pestova, T.V., Qian, S.B., and Jaffrey, S.R. (2015). 5′ UTR m(6)A promotes cap-independent translation. Cell *163*, 999–1010.

Moerke, N.J., Aktas, H., Chen, H., Cantel, S., Reibarkh, M.Y., Fahmy, A., Gross, J.D., Degterev, A., Yuan, J., Chorev, M., et al. (2007). Small-molecule inhibition of the interaction between the translation initiation factors eIF4E and eIF4G. Cell *128*, 257–267.

Pause, A., Belsham, G.J., Gingras, A.C., Donzé, O., Lin, T.A., Lawrence, J.C., Jr., and Sonenberg, N. (1994). Insulin-dependent stimulation of protein synthesis by phosphorylation of a regulator of 5′-cap function. Nature *371*, 762–767.

Paytubi, S., Morrice, N.A., Boudeau, J., and Proud, C.G. (2008). The N-terminal region of ABC50 interacts with eukaryotic initiation factor eIF2 and is a target for regulatory phosphorylation by CK2. Biochem. J. *409*, 223–231.

Paytubi, S., Wang, X., Lam, Y.W., Izquierdo, L., Hunter, M.J., Jan, E., Hundal, H.S., and Proud, C.G. (2009). ABC50 promotes translation initiation in mammalian cells. J. Biol. Chem. *284*, 24061–24073.

Pisarev, A.V., Hellen, C.U., and Pestova, T.V. (2007). Recycling of eukaryotic posttermination ribosomal complexes. Cell *131*, 286–299.

Scheuner, D., Song, B., McEwen, E., Liu, C., Laybutt, R., Gillespie, P., Saunders, T., Bonner-Weir, S., and Kaufman, R.J. (2001). Translational control is required for the unfolded protein response and in vivo glucose homeostasis. Mol. Cell *7*, 1165–1176.

Schütz, P., Bumann, M., Oberholzer, A.E., Bieniossek, C., Trachsel, H., Altmann, M., and Baumann, U. (2008). Crystal structure of the yeast eIF4A-eIF4G complex: an RNA-helicase controlled by protein-protein interactions. Proc. Natl. Acad. Sci. USA *105*, 9564–9569.

Schwartz, S., Mumbach, M.R., Jovanovic, M., Wang, T., Maciag, K., Bushkin, G.G., Mertins, P., Ter-Ovanesyan, D., Habib, N., Cacchiarelli, D., et al. (2014). Perturbation of m6A writers reveals two distinct classes of mRNA methylation at internal and 5′ sites. Cell Rep. *8*, 284–296.

Shi, H., Wang, X., Lu, Z., Zhao, B.S., Ma, H., Hsu, P.J., Liu, C., and He, C. (2017). YTHDF3 facilitates translation and decay of N(6)-methyladenosine-modified RNA. Cell Res. *27*, 315–328.

Sonenberg, N., and Hinnebusch, A.G. (2007). New modes of translational control in development, behavior, and disease. Mol. Cell *28*, 721–729.

Sonenberg, N., and Hinnebusch, A.G. (2009). Regulation of translation initiation in eukaryotes: mechanisms and biological targets. Cell *136*, 731–745.

Starck, S.R., Jiang, V., Pavon-Eternod, M., Prasad, S., McCarthy, B., Pan, T., and Shastri, N. (2012). Leucine-tRNA initiates at CUG start codons for protein synthesis and presentation by MHC class I. Science *336*, 1719–1723.

Terenin, I.M., Andreev, D.E., Dmitriev, S.E., and Shatsky, I.N. (2013). A novel mechanism of eukaryotic translation initiation that is neither m7G-cap-, nor IRES-dependent. Nucleic Acids Res. *41*, 1807–1816.

Thoreen, C.C., Kang, S.A., Chang, J.W., Liu, Q., Zhang, J., Gao, Y., Reichling, L.J., Sim, T., Sabatini, D.M., and Gray, N.S. (2009). An ATP-competitive mammalian target of rapamycin inhibitor reveals rapamycin-resistant functions of mTORC1. J. Biol. Chem. *284*, 8023–8032.

Thoreen, C.C., Chantranupong, L., Keys, H.R., Wang, T., Gray, N.S., and Sabatini, D.M. (2012). A unifying model for mTORC1-mediated regulation of mRNA translation. Nature *485*, 109–113.

Tyzack, J.K., Wang, X., Belsham, G.J., and Proud, C.G. (2000). ABC50 interacts with eukaryotic initiation factor 2 and associates with the ribosome in an ATP-dependent manner. J. Biol. Chem. *275*, 34131–34139.

Wang, X., Zhao, B.S., Roundtree, I.A., Lu, Z., Han, D., Ma, H., Weng, X., Chen, K., Shi, H., and He, C. (2015). N(6)-methyladenosine modulates messenger RNA translation efficiency. Cell *161*, 1388–1399.

Wang, P., Doxtader, K.A., and Nam, Y. (2016a). Structural basis for cooperative function of Mettl3 and Mettl14 methyltransferases. Mol. Cell *63*, 306–317.

Wang, X., Feng, J., Xue, Y., Guan, Z., Zhang, D., Liu, Z., Gong, Z., Wang, Q., Huang, J., Tang, C., et al. (2016b). Structural basis of N(6)-adenosine methylation by the METTL3-METTL14 complex. Nature *534*, 575–578.

Warner, J.R. (1999). The economics of ribosome biosynthesis in yeast. Trends Biochem. Sci. *24*, 437–440.

Weingarten-Gabbay, S., Elias-Kirma, S., Nir, R., Gritsenko, A.A., Stern-Ginossar, N., Yakhini, Z., Weinberger, A., and Segal, E. (2016). Comparative genetics. Systematic discovery of cap-independent translation sequences in human and viral genomes. Science *351*, aad4939.

Wek, R.C., Jiang, H.Y., and Anthony, T.G. (2006). Coping with stress: eIF2 kinases and translational control. Biochem. Soc. Trans. *34*, 7–11.

Xue, S., Tian, S., Fujii, K., Kladwang, W., Das, R., and Barna, M. (2015). RNA regulons in Hox 5′ UTRs confer ribosome specificity to gene regulation. Nature *517*, 33–38.

Yanagiya, A., Suyama, E., Adachi, H., Svitkin, Y.V., Aza-Blanc, P., Imataka, H., Mikami, S., Martineau, Y., Ronai, Z.A., and Sonenberg, N. (2012). Translational homeostasis via the mRNA cap-binding protein, eIF4E. Mol. Cell *46*, 847–858.

Yang, Y., Fan, X., Mao, M., Song, X., Wu, P., Zhang, Y., Jin, Y., Yang, Y., Chen, L.L., Wang, Y., et al. (2017). Extensive translation of circular RNAs driven by N(6)-methyladenosine. Cell Res. *27*, 626–641.

Ye, J., Palm, W., Peng, M., King, B., Lindsten, T., Li, M.O., Koumenis, C., and Thompson, C.B. (2015). GCN2 sustains mTORC1 suppression upon amino acid deprivation by inducing Sestrin2. Genes Dev. *29*, 2331–2336.

Zhou, J., Wan, J., Gao, X., Zhang, X., Jaffrey, S.R., and Qian, S.B. (2015). Dynamic m(6)A mRNA methylation directs translational control of heat shock response. Nature *526*, 591–594.

Zoncu, R., Efeyan, A., and Sabatini, D.M. (2011). mTOR: from growth signal integration to cancer, diabetes and ageing. Nat. Rev. Mol. Cell Biol. *12*, 21–35.

STAR★METHODS

KEY RESOURCES TABLE

REAGENT or RESOURCE	SOURCE	IDENTIFIER
Antibodies		
Rabbit polyclonal anti-4EBP1	Cell Signaling Technology	Cat#9452L; RRID: AB_331692
Rabbit polyclonal Phospho-4E-BP1	Cell Signaling Technology	Cat #9459S; RRID: AB_330985
Rabbit monoclonal eIF4G-1 (clone D6A6)	Cell Signaling Technology	Cat#8701S; RRID: AB_11178378
Rabbit monoclonal RPS6 (clone 5G10)	Cell Signaling Technology	Cat#2217S; RRID: AB_331355
Rabbit polyclonal Phospho-RPS6	Cell Signaling Technology	Cat#2215S; RRID: AB_331682
Rabbit polyclonal S6K	Cell Signaling Technology	Cat#9202S; RRID: AB_331676
Rabbit polyclonal Phospho-S6K	Cell Signaling Technology	Cat#9205S; RRID: AB_330944
Rabbit polyclonal eEF2	Cell Signaling Technology	Cat#2332S; RRID: AB_10693546
Rabbit polyclonal Phospho-eEF2	Cell Signaling Technology	Cat#2331S; RRID: AB_10015204
Mouse monoclonal eIF4E (clone P-2)	Santa Cruz Biotechnology	Cat #sc-9976; RRID: AB_627502
Rabbit polyclonal ABCF1(clone H-135)	Santa Cruz Biotechnology	Cat #sc-98376; RRID: AB_2288921
Mouse monoclonal YTHDF3 (clone F-2)	Santa Cruz Biotechnology	Cat #sc-377119; RRID: AB_2687436
Rabbit polyclonal METTL3	Proteintech Group	Cat#15073-1-AP; RRID: AB_2142033
Rabbit polyclonal YTHDF2	Proteintech Group	Cat#24744-1-AP; RRID: AB_2687435
Rabbit polyclonalYTHDF1	Abcam	Cat# ab99080; RRID: AB_10675362
Mouse monoclonal β-actin	Sigma-Aldrich	Cat#A5441; RRID: AB_476744
Rabbit polyclonal METTL14	Sigma-Aldrich	Cat# HPA038002; RRID: AB_10672401
Mouse monoclonal Puromycin (4A12)	Developmental Studies Hybridoma Bank	Cat#PMY-2A4
Bacterial and Virus Strains		
DECIPHER pRSI9-U6-(sh)-UbiC-TagRFP-2A-Puro	Cellecta	N/A
Chemicals, Peptides, and Recombinant Proteins		
Torin1	Tocris Bioscience	Cat#4247
Thapsigargin	Sigma-Aldrich	T9033; CAS: 67526-95-8
Critical Commercial Assays		
EasyTag EXPRESS 35S Protein Labeling Mix	PerkinElmer	NEG772007MC
High Capacity cDNA Reverse Transcription Kit	Applied Biosystems	Cat#4368814
Power SYBR Green PCR Master Mix	Applied Biosystems	Cat#4368706
mMessage mMachine T7 Ultra kit	Ambion	Cat#AM1345
MEGAscript T7 Transcription Kit	Ambion	Cat#AM1334
Dynabeads Oligo(dT)25	Thermo Fisher Scientific	Cat#61005
Deposited Data		
Raw sequencing data	This paper	GEO: GSE101865
Re-analyzed m6A-seq data	Schwartz et al., 2014; Geula et al., 2015	GEO: GSE55575, GSE61998
Re-analyzed Ribo-seq data	Thoreen et al., 2012; Wang et al., 2015	GEO: GSE36892, GSE63591
Mouse genome, transcriptome, GRCm38.p4	Ensembl	http://www.ensembl.org/index.html
Experimental Models: Cell Lines		
Mus musculus: embryonic fibroblast cells	Laboratory of David J. Kwiatkowski	N/A

(*Continued on next page*)

Continued

REAGENT or RESOURCE	SOURCE	IDENTIFIER
Oligonucleotides		
shRNA targeting sequence: Abcf1_F: ACCGGCG CGGACAAAGTAGTGAAGAACTCGAGTTCTTCA CTACTTTGTCC GCGTTTTTTG	This paper	N/A
shRNA targeting sequence: Abcf1_R: CGAACAAA AAACGCGGACAAAGTAGTGAAGAACTCGAGTTC TTCACTAC TTTGTCCGCGC	This paper	N/A
shRNA targeting sequence: Mettl3_F: ACCGGGCT ACAGGATGACGGCTTTCTCTCGAGAGAAAGCCG TCATCCTG TAGCTTTTTTG	This paper	N/A
shRNA targeting sequence: Mettl3_R: CGAACAAAA AAGCTACAGGATGACGGCTTTCTCTCGAGAGAAA GCCGTC ATCCTGTAGCC	This paper	N/A
shRNA targeting sequence: Mettl14-1_F: ACCGGG GATCAAAGGAACCGTGAAGCCTCGAGGCTTCAC GGTTCCTTT GATCCTTTTTTG	This paper	N/A
shRNA targeting sequence: Mettl14-1_R: CGAACAA AAAAGGATCAAAGGAACCGTGAAGCCTCGAGGCT TCACGG TTCCTTTGATCCC	This paper	N/A
shRNA targeting sequence: Mettl14-2_F: ACCGGG GGAGAGTATGCTTGCGAAAGCTCGAGCTTTCGC AAGCATACTC TCCCTTTTTTG	This paper	N/A
shRNA targeting sequence: Mettl14-2_R: CGAACAA AAAAGGGAGAGTATGCTTGCGAAAGCTCGAGCTTT CGCAA GCATACTCTCCCC	This paper	N/A
DNA probes for RNA pull-down: Hsp70: 5′-biotin-TEG-TAAAAAGAAGAAATAGTCGTAAGATG-3′	This paper	N/A
DNA probes for RNA pull-down: β-actin: 5′-biotin-TEG-AAAAACAAATAAAGCCATGCCAATCTCA-3′	This paper	N/A
Recombinant DNA		
Plasmid: GST-METTL3 (PGEX-6p-1)	This paper	N/A
Plasmid: GST-eIF4E (PGEX-6p-1)	This paper	N/A
Plasmid: SBP-METTL3 (pcDNA3.1)	This paper	N/A
Software and Algorithms		
Bowtie	Langmead et al., 2009	http://bowtie-bio.sourceforge.net/index.shtml
Cutadapt	Martin, 2011	http://cutadapt.readthedocs.io/en/stable/index.html
MEME	Bailey et al., 2009	http://meme-suite.org
Perl	Perl	https://www.perl.org

CONTACT FOR REAGENT AND RESOURCE SHARING

Further information and requests for resources and reagents should be directed to and will be fulfilled by the Lead Contact Shu-Bing Qian (sq38@cornell.edu).

EXPERIMENTAL MODEL AND SUBJECT DETAILS

Cell Lines and Reagents

HeLa cells and MEF cells were maintained in Dulbecco's Modified Eagle's Medium (DMEM) with 10% fetal bovine serum (FBS). Starvation media was based on Hank's Balanced Salt Solution (HBSS) supplemented with 10% dialyzed FBS. Cycloheximide (#C7698-5G) and puromycin (#P7255-250MG) were purchased from Sigma Aldrich. Torin1 (#4247) was purchased from Tocris

Bioscience and dissolved in DMSO. [^{35}S]-methionine was purchased from PerkinElmer (#NEG772007MC). m7GTP beads for cap pulldown experiments were purchased from Jena Biosciences (AC-155).

Lentiviral shRNAs

All shRNA targeting sequences were cloned into DECIPHER pRSI9-U6-(sh)-UbiC-TagRFP-2A-Puro (Cellecta, CA). shRNA targeting sequences listed below were based on RNAi consortium at Broad Institute (https://www.broad.mit.edu/rnai/trc). Lentiviral particles were packaged using Lenti-X 293T cells (Clontech). Virus-containing supernatants were collected at 48-h after transfection and filtered to eliminate cells. MEF cells were infected by the lentivirus for 48 hr before selection by 2 μg ml^{-1} puromycin.

METHOD DETAILS

Puromycin Labeling

Cells were treated with HBSS + dFBS for 50 minutes before media was changed to HBSS + dFBS supplemented with 10 μM puromycin for an additional ten minutes. Cells were washed twice with ice-cold PBS and lysed with 1 × SDS before proteins were separated using SDS-PAGE.

[^{35}S] Radiolabeling

MEF cells were briefly incubated in methionine- and cysteine-free media before addition of 50 μCi of [^{35}S]-methionine. Labeling was stopped by ice-cold DMEM containing 100 μM of cycloheximide. Cells were washed with PBS containing 100 μM of cycloheximide, and lysed with polysome lysis buffer. For the quantitation of [^{35}S]-Met-labeled proteins, cell lysates were resolved on a 10% Tris-Glycine SDS-PAGE and radiography captured by Typhoon 9400. Quantification of [^{35}S] methionine incorporation was done using ImageJ software. For scintillation counting, samples were precipitated by 10% trichloroacetic acid (TCA). The mixture was heated for 10 min at 90°C and then chilled on ice for 10 min. The precipitates were collected on GF/C filter membrane (Watman) and the [^{35}S] incorporation was measured by scintillation counting (Beckman).

Cap Pull-Down

One 10 cm dish of cells was seeded at 70% confluency and incubated overnight at 37°C. Cells were then washed with ice-cold PBS and lysed with 500 μL polysome buffer supplemented with 1% NP-40 (v/v) and protease inhibitors. Dishes were scraped and cell lysates were clarified at 4°C for 10 minutes at 10,000 g. 750 μL of lysate supernatant was added to m^{7}GTP beads that had been washed three times with 1 mL polysome buffer supplemented with 0.1% NP-40 (v/v) followed by incubation at 4°C for 1 hour. Beads were then washed three times with polysome buffer at 4°C. 4 × SDS buffer was added directly to beads after the final wash followed by immunoblotting.

Immunoblotting

Cells were lysed on ice in TBS buffer (50 mM Tris, pH7.5, 150 mM NaCl, 1 mM EDTA) containing protease inhibitor cocktail tablet, 1% Triton X-100, and 2 U ml^{-1} DNase. After incubating on ice for 30 min, the lysates were heated for 10 min in SDS/PAGE sample buffer [50 mM Tris (pH6.8), 100 mM dithiothreitol, 2% SDS, 0.1% bromophenol blue, 10% glycerol). Proteins were separated on SDS-PAGE and transferred to Immobilon-P membranes (Millipore). Membranes were blocked for 1-h in TBS containing 5% non-fat milk and 0.1% Tween-20, followed by incubation with primary antibodies overnight at 4°C. After incubation with horseradish peroxidase-coupled secondary antibodies at room temperature for 1 h, immunoblots were visualized using enhanced chemiluminescence (ECL^{Plus}, GE Healthcare).

mRNA Pull-Down Using DNA Probes

To isolate β-actin and Hsp70 mRNAs, we adapted a previously published method (Starck et al., 2012). In brief, DNA oligos were designed to complement to the 3′ ends of β-actin or Hsp70 mRNAs and synthesized by conjugating with biotin at the 5′ end. Cells were lysed using lysis buffer (20 mM Tris-Cl (pH 8.0), 5 mM $MgCl_2$, 100 mM NaCl, 2 mM DTT, 8% sucrose, and 1% NP-40 (v/v)) followed by incubation with DNA oligos at 4°C for 1 hour. Streptavidin beads were added to capture endogenous mRNAs and the associated proteins.

Mass Spectrometry

Samples were processed for mass spectrometry by Cornell's Proteomics & Mass Spectrometry Facility. Briefly, samples were desalted and normalized for protein content using a gel-based method. Proteins were digested using trypsin and the generated peptides were analyzed using an Orbitrap nanoLC-MS/MS 90-120 minute gradient. Mascot software was used to map identified peptides to proteins can calculate relative peptide scores.

Real-Time PCR

Total RNA was isolated by TRIzol reagent (Invitrogen) and reverse transcription was performed using High Capacity cDNA Reverse Transcription Kit (Invitrogen). Real-time PCR analysis was conducted using Power SYBR Green PCR Master Mix (Applied Biosystems) and carried on a LightCycler 480 Real-Time PCR System (Roche Applied Science).

In Vitro Transcription

Plasmids containing the corresponding 5′ untranslated region sequences of mouse *HSPA1A* and full length firefly luciferase were used as templates. Transcripts with normal m^7G cap were generated using the mMessage mMachine T7 Ultra kit (Ambion) and transcripts with non-functional cap analog GpppA were synthesized using MEGAscript T7 Transcription Kit (Ambion). To obtain mRNAs with the adenosine replaced with m^6A, *in vitro* transcription was conducted in a reaction in which 5% of the adenosine was replaced with N^6-methyladenosine. All mRNA products were purified using the MEGAclear kit (Ambion) according to the manufacturer's instruction.

Real-Time Luciferase Assay

Cells grown in 35 mm dishes were transfected with *in vitro* synthesized mRNA containing the luciferase gene. Luciferase substrate D-luciferin (1 mM, Regis Tech) was added into the culture medium immediately after transfection. Luciferase activity was monitored and recorded using Kronos Dio Luminometer (Atto).

Electrophoretic Mobility Shift Assay

Electrophoretic mobility shift assay was performed as previously described (Alarcón et al., 2015). The m^6A-modified or -unmodified RNA probe was synthesized by Thermo Scientific with the sequence of 5′- CGAUCCUCGGCCAGGXCCAGCCUUCCCCA-3′ (X = A or m^6A). The capped or non-capped mRNA (Hsp70-5′UTR) was synthesized using the mMessage mMachine T7 Ultra kit (Ambion). The probe was labeled in a 50ul reaction mixture containing 2 μl RNA probe (1 μM), 5 μl 10 × T4 PNK buffer (NEB), 1 μl T4 PNK (NEB), 40 U ml^{-1} RNaseOUT (Thermo Scientific), 1 μl [^{32}P]ATP and 40 μl RNase-free water at 37°C for 1 h. The labeled probe was then purified by RNase-free micro bio-spin columns with bio-gel P30 (Bio-Rad 732-6250) according to manufacturer's protocols. After adding 2.5 μl 20 × SSC (Promega) buffer, the RNA was denatured at 65°C for 10 min and slowly cooled down. The purified probe (20 fmol) was incubated with increasing amount of GST-METTL3 at 4°C for 1 h in binding buffer containing 10 mM HEPES, pH 8.0, 50 mM KCl, 1 mM EDTA, 0.05% Triton X-100, 5% glycerol, 10 μg ml^{-1} salmon DNA, 1 mM DTT and 40 U ml-1 RNaseOUT (Thermo Scientific). The RNA-protein mixture was loaded on Novex 8% TBE gel and run at 100 V at 4°C. The signal was recoded via autoradiography.

Recombinant Protein Purification and *In Vitro* Cap-Binding Assay

Mettl3 and *Eif4e* coding sequences were cloned into pGEX-6P-1 vector using the primers as follows: METTL3-F, 5′-ACGCGTC GACTCATGTCGGACACGTGGAGCTC-3′; METTL3-R, 5′- ATAAGAATGCGGCCGCCTATAAATTCTTAGGTTTAG-3′; eIF4E-F, 5′- GCGAATTCATGGCGACTGTCGAACCGGA-3′; eIF4E-R, 5′-CCGCTCGAGTTAAACAACAAACCTATTTTTAG-3′. The constructs were transformed into the *E. coli* bacteria BL21. After inducing the fusion protein expression at 20°C for 3-4 h in the presence of 0.5 mM IPTG, cells were collected and lysed in PBS lysis buffer supplemented with 0.5 mM PMSF, 1 mM DTT, protease inhibitor cocktail (Roche), 0.1% (v/v) Triton X-100 and sonicated for 10 min. Cell debris was removed by centrifugation at 12,000 rpm for 30 min, the supernatant was mixed with 2 mL equilibrated Pierce glutathione agarose and incubated for 2-3 h at 4°C. The resin was washed five times and eluted in GST elution buffer (5mM glutathione, 50mM Tris-HCl (pH 8.0)).

Purified GST-METTL3 or GST-eIF4E protein was incubated with m^7GTP agarose beads (Jena Bioscience) in binding buffer (20 mM Tris-HCl, 100mM NaCl, 25mM MgCl2, 0.5% Nonidet P-40, and protease inhibitors) at 4°C for 2 h. Pelleted beads were washed four times with 0.5 mL of binding buffer and re-suspended in 0.6 mL of binding buffer supplemented with 1 mM GTP for another 1 h at 4°C. After washing with lysis buffer for four times, the beads were re-suspended in sample buffer and boiled for 5 min. m^7GTP-bound proteins, GTP wash and input (5% purified proteins) were loaded on 8% SDS-PAGE gels and subjected to western blot using anti-GST antibody (1:1000).

Immunofluorescence Staining

Cells grown on glass coverslips were fixed in 4% paraformaldehyde for 10 min at room temperature. After permeabilization in 0.2% Triton X-100 for 5 min at room temperature, the coverslips were washed by PBS for three times and then blocked with 1% BSA for 30 min. Cells were stained with indicated primary antibody overnight at 4°C, followed by incubation with Alexa Fluor 546 donkey anti-mouse secondary antibody or Alexa Fluor 546 donkey anti-rabbit secondary antibody for 1 h at room temperature. The nuclei were counter-stained with Hechest (1:1000) for 10 min. Coverslips were mounted onto slides and visualized using a Zeiss LSM710 confocal microscope.

Co-immunoprecipitation Assay

HEK293 cells (one 10-cm plate) transfected with SBP-tagged METTL3 only or SBP-tagged METTL3 with ABCF1-myc plasmids for 24 h. The transfected cells were subjected to amino acid starvation for 2 h or with heat shock stress (42°C) for 1 h followed by recovery

at 37°C for 2 h. Cells were collected by centrifuge at 1000 rpm for 5 min. The cell pellet was lysed in lysis buffer (150 mM KCl, 10 mM HEPES (pH 7.6), 1 mM EDTA, 0.5% NP-40, 0.5 mM DTT and protease inhibitor cocktail) and rotated at 4°C for 30 min. The cell debris was removed by centrifugation at 14,000 rpm for 15 min. The supernatant was incubated with streptavidin magnetic beads in lysis buffer for 3-4 h at 4°C. The beads were collected by magnetic stand, and the supernatant was saved as the fraction of flow through. Subsequently the beads were washed with 1 mL wash buffer (200 mM NaCl, 50 mM HEPES (pH 7.6), 1 mM EDTA and 0.05% NP-40, 0.5 mM DTT, protease inhibitor cocktail) for 6 times. SDS buffer was directly added in the beads and boiled for 5 min. The samples were loaded on 8% SDS-PAGE gels and subjected to western blot using indicated antibodies.

m^{6}A Dot Blot

mRNA was purified from total RNA using Dynabeads Oligo(dT)25 (Thermo Fisher). Equal amounts of mRNA were spotted to a nylon membrane (Fisher), followed by UV crosslinking at UV 254 nm, 0.12 J/cm^2. After blocking in PBST containing 5% non-fat milk and 0.1% Tween-20 for 1 hr, the membrane was incubated with 1:1000 diluted anti-m^{6}A antibody overnight at 4°C. The membrane was incubated with HRP-conjugated anti-rabbit IgG (1:5000 dilution) for 1 hr and visualized by using enhanced chemiluminescence (ECLPlus, GE Healthcare).

Polysome Profiling Analysis

Sucrose solutions were prepared in polysome buffer (10 mM HEPES, pH 7.4, 100 mM KCl, 5 mM $MgCl_2$, 100 μg ml^{-1} cycloheximide and 2% Triton X-100). A 15%- 45% (w/v) Sucrose density gradients were freshly prepared in SW41 ultracentrifuge tubes (Backman) using a Gradient Master (BioComp Instruments). Cells were pre-treated with 100 μg ml^{-1} cycloheximide for 3 min at 37°C followed by washing using ice-cold PBS containing 100 μg ml^{-1} cycloheximide. Cells were then lysed in polysome lysis buffer. Cell debris were removed by centrifugation at 14,000 rpm for 10 min at 4°C. 500 μl of supernatant was loaded onto sucrose gradients followed by centrifugation for 2 h 28 min at 38,000 rpm 4°C in a SW41 rotor. Separated samples were fractionated at 0.75 ml/min through an automated fractionation system (Isco) that continually monitores OD_{254} values. An aliquot of ribosome fraction were used to extract total RNA using Trizol LS reagent (Invitrogen) for real-time PCR analysis.

RNA-Seq and m^{6}A-Seq

For m^{6}A immunoprecipitation, total RNA was first isolated using Trizol reagent followed by fragmentation using freshly prepared RNA fragmentation buffer (10 mM Tris-HCl, pH 7.0, 10 mM $ZnCl_2$). 5 μg fragmented RNA was saved as input control for RNA-seq. 1 mg fragmented RNA was incubated with 15cμg anti-m^{6}A antibody (Millipore ABE572) in 1 × IP buffer (10cmM Tris-HCl, pH 7.4, 150cmM NaCl, and 0.1% Igepal CA-630) for 2chr at 4°C. The m^{6}A-IP mixture was then incubated with Protein A beads for additional 2chr at 4°C on a rotating wheel. After washing 3 times with IP buffer, bound RNA was eluted using 100cμl elution buffer (6.7 mM *N*^{6}-Methyladenosine 5′-monophosphate sodium salt in 1 × IP buffer), followed by ethanol precipitation. Precipitated RNA was used for cDNA library construction and high-throughput sequencing described below.

Ribo-Seq

Ribosome fractions separated by sucrose gradient sedimentation were pooled and digested with *E. coli* RNase I (Ambion, 750 U per 100 A260 units) by incubation at 4°C for 1 h. SUPERase inhibitor (50 U per 100 U RNase I) was then added into the reaction mixture to stop digestion. Total RNA was extracted using TRIzol reagent. Purified RNA was used for cDNA library construction and high-throughput sequencing described below.

cDNA Library Construction

Fragmented RNA input and m^{6}A-IP elutes were dephosphorylated for 1 hr at 37°C in 15 μl reaction (1 × T4 polynucleotide kinase buffer, 10 U SUPERase_In and 20 U T4 polynucleotide kinase). The products were separated on a 15% polyacrylamide TBE-urea gel (Invitrogen) and visualized using SYBR Gold (Invitrogen). Selected regions of the gel corresponding to 40-60 nt (for RNA-seq and m^{6}A-seq) or 25-35 nt (for Ribo-seq) were excised. The gel slices were disrupted by using centrifugation through the holes at the bottom of the tube. RNA fragments were dissolved by soaking overnight in 400 μL gel elution buffer (300 mM NaOAc, pH 5.5, 1 mM EDTA, 0.1 U/ml SUPERase_In). The gel debris was removed using a Spin-X column (Corning), followed by ethanol precipitation. Purified RNA fragments were re-suspended in nuclease-free water. Poly-(A) tailing reaction was carried out for 45 min at 37°C (1 × poly-(A) polymerase buffer, 1 mM ATP, 0.75 U/μl SUPERase_ In and 3 U *E. coli* poly-(A) polymerase).

For reverse transcription, the following oligos containing barcodes were used:

MCA02: 5′-pCAGATCGTCGGACTGTAGAACTCTCAAGCAGAAGACGGCATACGATTT TTTTTTTTTTTTTTTVN-3′;
LGT03: 5′-pGTGATCGTCGGACTGTAGAACTCTCAAGCAGAAGACGGCATACGATT TTTTTTTTTTTTTTTVN-3′;
YAG04: 5′-pAGGATCGTCGGACTGTAGAACTCTCAAGCAGAAGACGGCATACGATT TTTTTTTTTTTTTTTVN-3′;
HTC05: 5′-pTCGATCGTCGGACTGTAGAACTCTCAAGCAGAAGACGGCATACGATT TTTTTTTTTTTTTTTVN-3′.

In brief, the tailed-RNA sample was mixed with 0.5 mM dNTP and 2.5 mM synthesized primer and incubated at 65°C for 5 min, followed by incubation on ice for 5 min. The reaction mix was then added with 20 mM Tris (pH 8.4), 50 mM KCl, 5 mM $MgCl_2$,

10 mM DTT, 40 U RNaseOUT and 200 U SuperScript III. Reverse transcription reaction was performed according to the manufacturer's instruction. Reverse transcription products were separated on a 10% polyacrylamide TBE-urea gel as described earlier. The extended first-strand product band was expected to be approximately 100 nt, and the corresponding region was excised. The cDNA was recovered by using DNA gel elution buffer (300 mM NaCl, 1 mM EDTA). First-strand cDNA was circularized in 20 μL of reaction containing 1 × CircLigase buffer, 2.5 mM $MnCl_2$, 1M Betaine, and 100 U CircLigase II (Epicenter). Circularization was performed at 60°C for 1 h, and the reaction was heat inactivated at 80°C for 10 min. Circular single-strand DNA was re-linearized with 20 mM Tris-acetate, 50 mM potassium acetate, 10 mM magnesium acetate, 1 mM DTT, and 7.5 U APE 1 (NEB). The reaction was carried out at 37°C for 1 h. The linearized single-strand DNA was separated on a Novex 10% polyacrylamide TBE-urea gel (Invitrogen) as described earlier. The expected 100-nt product bands were excised and recovered as described earlier.

Deep Sequencing

Single-stranded template was amplified by PCR by using the Phusion High-Fidelity enzyme (NEB) according to the manufacturer's instructions. The oligonucleotide primers qNTI200 (5′-CAAGCAGAAGACGGCATA- 3′) and qNTI201 (5′-AATGATACGGCGAC CACCG ACAGGTTCAGAGTTCTACAGTCCGACG- 3′) were used to create DNA suitable for sequencing, i.e., DNA with Illumina cluster generation sequences on each end and a sequencing primer binding site. The PCR contains 1 × HF buffer, 0.2 mM dNTP, 0.5 μM oligonucleotide primers, and 0.5 U Phusion polymerase. PCR was carried out with an initial 30 s denaturation at 98°C, followed by 12 cycles of 10 s denaturation at 98°C, 20 s annealing at 60°C, and 10 s extension at 72°C. PCR products were separated on a nondenaturing 8% polyacrylamide TBE gel as described earlier. Expected DNA at 120 bp (for Ribo-seq), or 140 bp (for RNA-seq and m^6A-seq) was excised and recovered as described earlier. After quantification by Agilent BioAnalyzer DNA 1000 assay, equal amount of barcoded samples were pooled into one sample. Approximately 3–5 pM mixed DNA samples were used for cluster generation followed by deep sequencing by using sequencing primer 5′-CGACAGGTTCAGAGTTCTAC AGTCCGACGATC-3′ (Illumina HiSeq).

QUANTIFICATION AND STATISTICAL ANALYSIS

Preprocessing of Sequencing Reads

For Ribo-seq, the 3′ adaptor and low quality bases were trimmed by Cutadapt (Martin, 2011). The trimmed reads with length < 15 nucleotides were excluded. The remaining reads were mapped to the mouse transcriptome (ENSEMBL gene, GRCm38, longest CDS was selected if multiple transcripts existing) using Bowtie (Langmead et al., 2009) with parameters: -a -m1 –best –strata. Two mismatches are permitted. Non-uniquely mapped reads were disregarded for further analysis due to ambiguity. The same mapping procedure was applied to RNA-seq and m^6A-seq. For Ribo-seq, the 13^{th} position (12nt offset from the 5′ end) of the uniquely mapped read was defined as the ribosome ''P-site'' position. Uniquely mapped reads of Ribo-seq in the mRNA coding region were used to calculate the RPKM values for translation levels. For RNA-seq, uniquely mapped reads in the full length of mRNA were used to calculate the RPKM values. Transcripts with RPKM < 1 were excluded. Translation efficiency (TE) was defined as the ratio of Ribo-seq over RNA-seq.

Identification of m^6A Sites

We used a similar scanning strategy reported previously to identify m^6A peaks in the immunoprecipitation sample as compared to the input sample (Dominissini et al., 2012). In brief, for each ENSEMBL gene, a sliding window of 50 nucleotides with step size of 25 nucleotides was employed to scanning the longest isoform (based on CDS length; in the case of equal CDS, the isoform with longer UTRs was selected). Only transcripts in which the average coverage in immunoprecipitation is higher than 30 per kilo base were used in further analysis for reduction of background noise. For each window, a Peak-Over-Median score (POM) was derived by calculating the ratio of mean read coverage in the window to the median read coverage of the whole gene body. Windows scoring higher than 3 in the IP sample were obtained and all the resultant overlapping m^6A peak windows in the IP sample were iteratively clustered to infer the boundary of m^6A enriched region as well as peak position with maximal read coverage. Finally, a Peak-Over-Input (POI) score was assigned to each m^6A enriched region by calculating the ratio of POM in the IP sample to that in the input sample. A putative m^6A site was defined if the POI score was higher than 3. The peak position of each m^6A site was classified into three mutually exclusive mRNA structural regions including 5′ UTR, CDS, and 3′ UTR. For whole-transcript coverage plots, coverage at individual site was normalized by mean coverage of the transcript first, then each mRNA region was divided into 100 bins, coverages in the same bins were aggregated.

Motif Analysis

The 1000 m6A peaks with highest POI score were selected consensus motif finding. We used MEME Suite for motif analysis with parameters; -nmotifs3 -maxw6 –minw3 (Bailey et al., 2009). In brief, the flanking sequences of m^6A peaks (±40 nt) with POI scores were retrieved from mouse transcriptome and were used as MEME input.

DATA AND SOFTWARE AVAILABILITY

Statistical analysis was mainly done using GraphPad Prism and SigmaPlot (Systat Software). Unless otherwise noted, some analytical procedures were completed using custom Perl scripts. These scripts are available upon request. Deep sequencing data from Ribo-seq and RNA-seq have been deposited in the NCBI Gene Expression Omnibus database with accession code GEO: GSE101865. Original images can be found in Mendeley Data (https://doi.org/10.17632/9mrmpfb4y2.1).